A novel visco-elastic damage model for asphalt concrete and its numerical implementation

Peng Cao [a], Ph.D., Assistant Professor, Zhen Leng[b], Ph.D., Assistant Professor, Feiting Shi[c], Changjun Zhou[d*], Ph.D., Associate Professor, Zhifei Tan[e], Ziyu Wang[f]

[a] College of Architecture and Civil Engineering, Beijing University of Technology, Beijing, 100124 China, Email: caopeng518888@126.com

[b] Department of Civil and Environmental Engineering, The Hong Kong Polytechnic University, Hung Hom, Kowloon, Hong Kong, Tel: (+852) 2766 6007, Fax: (+852) 2334 6389, Email: zhen.leng@polyu.edu.hk

[c] School of Civil Engineering, Harbin Institute of Technology, Harbin, 150090 China. Email: shifeiting@sina.com

[d*]Corresponding author, School of Transportation and Logistics, Dalian University of Technology, Dalian, 116024, China. Email: zhouchangjun@dlut.edu.cn

[e] Department of Civil and Environmental Engineering, The Hong Kong Polytechnic University, Hung Hom, Kowloon, Hong Kong, Email: zhifeitan@gmail.com

[f] Hainan Tropical Ocean University, School of ecological environment, Sanya, Hainan 572022, China. Email: iamwziyu@163.com

Abstract: The creep of asphalt and asphalt concrete were numerically studied extensively. However, most of the previous studies only researched the decelerated creep stage and equi velocity creep stage while rarely shed light on the accelerated creep stage. This paper proposes a novel 3 dimensional visco-elastic damage model utilizing two spring and one dashpot components coupled with Kachanov and Robotnov (K-R) creep damage theory to describe the whole stages of the creep of asphalt and asphalt concrete, i.e., decelerated creep stage, equi-velocity creep stage, and accelerated creep stage. The damage evolution equation based on the K-R creep damage theory is integrated into the visco-elastic constitutive model by the continuum mechanics, and then the uniaxial creep damage solution is deducted. A robust numerical algorithm of this model is developed. Through numerical tests on uniaxial

compression and pre-notched three-point bending beam, the numerical curves are analogue to measured creep curves, which justifies the accuracy and efficiency of the visco-elastic model coupling with K-R creep damage theory and the corresponding numerical algorithm. This paper provides not only an accurate and robust creep damage constitutive model for the asphalt and asphalt concrete, but also a valuable model and an efficient numerical method to evaluate the damage and rupture behavior of large-scale infrastructures fabricated by asphalt and asphalt concrete.

Keywords: asphalt concrete, visco-elastic, K-R creep damage theory, finite element method

1. Introduction

Asphalt concrete can be classified as a composite material that consists of at least three components, including aggregate, asphalt mastic, and void. Asphalt plays a leading role in determining the mechanics performance such as creep deformation and stress relaxation. Due to the relaxation and diffusion of the long chain hydrocarbon in the asphalt mastic, the asphalt concrete always manifests the visco-elastic and visco-plastic behavior under sustained loading [1-3]. Definitely, the visco-elastic and visco-plastic behavior is an essential property of the asphalt concrete [4-5]. The visco-elastic behavior and plastic behavior of the asphalt extremely contributes to the permanent deformation of asphalt concrete such as rutting, which shortens the service life of asphalt pavement, involving extra cost for pavement maintenance [6-7].

The creep of asphalt concrete can mainly be divided into three stages, including decelerated creep stage, equi-velocity creep stage, and accelerated creep stage [8]. In the three stages, the decelerated creep stage arises in the initial loading and sustains the shortest time. Then the equi-velocity creep stage sustains the longest times, in which the sustained period is always determined by the loading amplitude and condition temperature. Actually, the accelerated creep stage is crucial in determining the damage and failure of the asphalt concrete. In this stage, the asphalt concrete mechanical properties change dramatically, inducing the complicated and involved

responses under external loading condition. Meanwhile, a notable phenomenon in this stage is that the deformation rate will increase rapidly and sustain to the ultimate fracture. When a material reaches the accelerated creep stage, it can be claimed that the material will lose the loading capacity immediately [9]. Thus, in asphalt mixture design, it is rational to just take the first two stages into account and neglect the accelerated creep stage. Abundant researches have paid more attention to the asphalt concrete behavior under creep state in the first two stages. Traditional visco-elastic models [10-12] with the damping and elastic components provided effective and accurate methods for analyzing the first two stages creep defamation. The most popular models are the burgers model [13], the generalized Kelvin model and the generalized Maxwell model [14-16]. These traditional models [10-16] utilized parallel connection and series connection method with the damping, elastic and slip components to fit creep curves and back-calculate the parameters of these damping and elastic components, providing the energy dissipation and instantaneous response, respectively [17]. The accelerated creep stage is different from the first two stages with the rapid damage accumulation phenomenon. Groups of the crazes formed in the first two stages commence to interact and intersect with each other, prompting the fracture in the material [18]. Therefore, the traditional visco-elastic and visco-plastic models are not applicable for the accelerated creep stage since they are lack of the damage evolution description. How to establish a rational damage mechanism and transfer it into traditional visco-elastic and visco-plastic models is still an involved and sophisticated problem [19-20]. Consequently, the nonlinear behavior in the accelerate creep stage makes the task developing nonlinear visco-elastic and plastic models are of great necessity.

Based on the Schapery's pseudo strain postulated theory, Kim and Little [21] and Park et al. [22] developed a visco-elastic model coupled with damage factor in term of the continuum mechanics frame. This model provided an alternate to estimate the failure behavior of the asphalt material under creep condition. Subsequently, Darabi, et al. [23-24] proposed a visco-elastic-plastic damage model for asphalt concrete, in which the temperature influence can be taken in account, due to the thermodynamic

foundation of the model. Shahsavari et al. [25] presented a phenomenological viscoelastic–viscoplastic–viscodamage constitutive model, developed within the framework of irreversible thermodynamics. Judycki [26] proposed a nonlinear visco-elastic model with nonlinear slip components for analyzing the creep deformation of the modified asphalt concrete material, in which the damage behavior is imported skillfully by means of the nonlinear slip components. Zhang et al. [27] proposed a one dimensional (1D) visco-elastic coupled damage mode for describing the three creep stages with analytic method [28]. Through the continuum mechanics damage theory, Zheng et al. [29-30] developed a series of visco-elastic-plastic damage models to simulate the creep behavior of asphalt concrete under various loading and temperature conditions. Lu and Wright [31] proposed a nonlinear visco-plastic model and integrated this model into the numerical method for predicting the three creep deformation stages and ultimate failure of asphalt binder.

Ye and Chen [32-33] also developed the visco-elastic coupled damage model to simulate the creep behavior of asphalt concrete. Cao et al. [34-35] developed a nonlocal visco-damage model using the area weighted method to simulate the damage and softening behavior of asphalt concrete. Bandyopadhyaya et al. [36] simulated the asphalt concrete with random aggregate technique. The damage mechanism also exists in the fatigue of asphalt and asphalt concrete [37]. Hafeez et al. [38] and Castro and Sanchez [39] analyzed the fatigue failure of asphalt concrete and attributed the damage mechanism to the reduction in stiffness modulus. Zeng et al. [40] developed a 1D creep damage model based on the K-R creep damage constitutive model for predicting the three-stage creep behavior of asphalt binder. Unfortunately, their work focuses on the 1D condition and the uniaxial stress is the only variable attaching to the damage evolution.

From the literature above, it is obviously found that many efforts have been devoted to developing and applying the visco-elastic and visco-plastic model coupled with damage theory. The experiments are mainly uniaxial tension and compression creep test under loading condition and numerical approaches mainly use 1D constitutive model. Very few researches provided the accurate and effective three

dimensional (3D) model and the efficient and robust numerical algorithm, which limits their application. Actually, the in-situ condition of asphalt concrete material is under 3D loading states. Therefore, it is reasonable to conclude that 1D visco-elastic damage model derived from uniaxial creep test may provide little help to understand the creep behavior of asphalt concrete under 3D loading states. Furthermore, when the visco-elastic component and damage variables are considered, analytic solutions can only be obtained in a few load and boundary conditions. It is necessary to count on the numerical method and develop powerful numerical solution algorithms.

The objective of this study is to investigate the creep behavior of asphalt concrete with a novel 3 dimensional visco-elastic damage model utilizing two spring and one dashpot components coupled with Kachanov and Robotnov (K-R) creep damage theory. The corresponding numerical algorithm is developed and employed through integrating this constitutive model in the finite element method via a user defined subroutine.

2 Theoretical model

2.1 Three-element viscoelastic model

The three-element viscoelastic model (Fig.1) includes a spring and a Kelvin model (short for 2S1D model), and responses to the load instantaneously. Definitely, the asphalt and asphalt concrete manifest the solid characteristic, thus 2S1D model is suitable for evaluating the creep response. This model was adopted and modified with damage mechanism in the creep behavior of asphalt binder [40]. Now we start to deduce the solution of this model for 1D condition. When the system is under fixed stress loading with magnitude σ, the equilibrium equation can be written as Eq. (1).

$$\begin{cases} \varepsilon = \varepsilon_1 + \varepsilon_2 \\ \sigma = E_2\varepsilon_2 \\ \sigma = E_1\varepsilon_1 + \eta_1\dot{\varepsilon}_1 \end{cases} \tag{1}$$

where, ε is the total strain; ε_1 and ε_2 are strains from the Kelvin and spring components, respectively; E_1 and E_2 are the stiffness of the Kelvin and spring

components, respectively; $\dot{\varepsilon}_1$ and η_1 are the damping coefficient and rate of the strain ε_1, respectively.

Through the Laplace transformation, Eq. (1) can be written as:

$$\begin{cases} \overline{\varepsilon} = \overline{\varepsilon}_1 + \overline{\varepsilon}_2 \\ \overline{\sigma} = E_2 \overline{\varepsilon}_2 \\ \overline{\sigma} = E_1 \overline{\varepsilon}_1 + \eta_1 s \overline{\varepsilon}_1 \end{cases} \tag{2}$$

The superscript "¯" represents the variable in the Laplace coordinate, and the variable s is the Laplace factor.

With the σ eliminated, we can get:

$$\overline{\sigma} / (E_1 + \eta_1 s) + \overline{\sigma} / E_2 = \overline{\varepsilon}_1 + \overline{\varepsilon}_2 = \overline{\varepsilon} \tag{3}$$

Through the inverse Laplace transformation, we can get the constitutive model from the 1D condition to 3D condition as Eq. (4).

$$\sigma_{ij}(t) = \int_0^t E_{ijkl} \dot{\varepsilon}_{kl}^0 \exp[-\frac{t-\tau}{\tau_0}] d\tau = \dot{\varepsilon}_{kl}^0 \int_0^t E_{ijkl} \exp[-\frac{t-\tau}{\tau_0}] d\tau \tag{4}$$

where, t represents time, τ represents the reduced time, $\dot{\varepsilon}_{kl}^0$ represents the strain under the deflection load, $E_{ijkl}(t)$ represents the relaxation modulus, which can be obtained from the three-component model from Bergstrom [41].

However, in complicated boundary conditions or time-dependent conditions, Eq. (4) cannot be solved with the analytic method, especially for the 3D conditions. Actually, the numerical method is a better option for most conditions.

The integration of Eq. (4) yields to Eq. (5a):

$$\sigma_{ij}(t) = E_{ijkl}(0) \varepsilon_{kl}(t) + \int_0^t \varepsilon_{kl}(t-\tau) \frac{dE_{ijkl}(\tau)}{d\tau} d\tau \tag{5a}$$

When the applied load meets the requirement $\varepsilon_{ij}(t) = \begin{cases} 0, & \text{if } t < 0 \\ \dot{\varepsilon}_{ij}^0 \cdot t, & \text{if } t \geq 0 \end{cases}$, while $E_{ijkl}(t)$ can be expanded to power series, then the Eq. (5a) can be written as Eq. (5b).

$$\sigma_{ij}(t)=\int_0^t E_{ijkl}(0)\dot{\varepsilon}_{kl}^0 \exp[-\frac{t-\tau}{\tau_0}]d\tau \tag{5b}$$

Only the first order derivative of the variables exists in Eq. (5b), which will simplify the numerical solution procedure with the traditional numerical difference methods such as the forward Euler method, the backward Euler method, and the central difference method. If the number of damping components rises, the higher order derivatives of the variables will rise, in which the above-mentioned difference numerical methods will reduce their general capacity to solve the constitutive equation. Then the specialized difference numerical method will be required. The difference numerical methods mentioned above have been provided in the most finite element platforms due to the universal and accurate capacity. Thereby, the 3D viscoelastic solid constitutive model proposed in this paper can be easily integrated for numerical applications. It is acknowledged that the 3D visco-elastic solid constitutive model is more suitable and accurate for numerical solution and application as other complicated models require the aid of various kinds of Runge-Kutta methods, in which the parameters changes from case to case.

2.2 K-R creep damage constitutive model

Kachanov firstly proposed the creep damage model for the long-term damage and failure behaviors of the metal material [42]. Kachanov [43] developed Robotnov's model [44] to form K-R creep damage constitutive model, which can evaluate the creep failure. Abundant researches adopted this model to explain the creep damage phenomena in the asphalt and asphalt concrete. A modified K-R creep damage on the basis of Zeng et al. [40] is deducted as follows.

The damage evolution equation defined by K-R is listed as:

$$\dot{\omega}=\frac{A\sigma_r^n}{(1-\omega)^m} \tag{6}$$

where, ω and $\dot{\omega}$ are the damage variable and the rate of damage variable, respectively. σ_r are the stress in the loading axial. A, m, and n are the material parameters responding to the damage evolution, respectively.

In 3D load condition, the suitable equivalence stress is necessary. Actually, different definitions of the equivalence stress will deduce various modified 3D K-R creep damage models [45-46]. In this paper, a new equivalence stress (Eq. (7)) [47] is formed from the J_2 stress and the maximal principal stress, which can consider the influences of the maximal principal stress and the shear stress on the creep behavior of asphalt materials. And the definition is shown as:

$$\sigma_{\mathrm{eq}} = \alpha\sigma_1 + (1-\alpha)J_2 \tag{7}$$

$$J_2 = \frac{1}{6}\sqrt{(\sigma_1-\sigma_2)^2 + (\sigma_1-\sigma_3)^2 + (\sigma_2-\sigma_3)^2} \tag{8}$$

where, α is the weighted parameters ranging from 0 to 1.0. When α equals to 1, the equivalence stress will degenerate into the uniaxial loading condition. σ_1, σ_2, and σ_3 are three principal stresses, respectively.

Based on Yu and Feng [42], the evolution equation of the damage is defined as:

$$\frac{\mathrm{d}\omega}{\mathrm{d}t} = \frac{A\sigma_{eq}^n}{(1-\omega)^m} \tag{9}$$

The solution can be deducted as:

$$\int_{\omega_0}^{\omega}(1-\omega)^m\,\mathrm{d}\omega = \int_0^t A\sigma_{eq}^n\mathrm{d}t \tag{10}$$

$$-\frac{(1-\omega)^{1+m}}{1+m}\Bigg|_{\omega_0}^{\omega_u} = A\sigma_{eq}^n\Big|_{t_0}^{t_f} \tag{11}$$

Consider the initial condition that ω_0, ω_u, and t_0 equal to 0, 1 and 0, respectively, from Eq. (11) we can obtain the ultimate failure time as Eq. (12).

$$t_f = [(1+m)A\sigma_{eq}^n]^{-1} \tag{12}$$

A life factor is defined as $\phi = [1-\frac{t}{t_f}]^{1/(m+1)}$, and the ϕ equals to 0 and 1 in the perfect condition and ultimate damage condition, respectively. The damage variable and its evolution equation can be obtained as Eq. (13) by means of life factor.

$$\omega = 1-\phi = 1-[1-\frac{t}{t_f}]^{1/(m+1)} \tag{13}$$

The strain equivalence theory proposed by Lematire and Chaboche [47] was used to update stresses in the effective space with the damage variable, ω. Based on the strain equivalence theory, the strain in perfect material caused by the stress $\tilde{\sigma}$ implemented in the effective space should be equivalent to the one in damage material caused by the stress σ implemented in the nominal stress space, as shown in Fig. 2. The symbol D in Fig. 2 represents the damage factor in material. By means of the strain equivalence theory, Eqs. (14-15) are shown below.

$$\varepsilon_{ij} = \frac{\sigma_{ij}}{\tilde{E}_{ijkl}} = \frac{\tilde{\sigma}_{ij}}{E_{ijkl}} = \frac{\sigma_{ij}}{(1-\omega)E_{ijkl}} \tag{14}$$

or

$$\sigma_{ij} = E_{ijkl}(1-\omega)\varepsilon_{kl} \tag{15}$$

When the material is under the 3D load condition, the constitutive equation in the effective space is defined as:

$$\varepsilon_{kl} = \frac{\sigma_{ij}}{\tilde{E}_{ijkl}} \tag{16}$$

where, the $\tilde{E}_{ijkl}$ and E_{ijkl} are the 4 order stiffness tensors in the nominal and effective space, respectively. And the damage variable is utilized to describe the degradation of the material stiffness as Eq. (17).

$$\omega = 1 - \frac{\tilde{E}_{ijkl}}{E_{ijkl}} \tag{17}$$

3 Numerical algorithms

When the material is in the elastic state, the lame constants are always utilized for defining the constitutive relationship between the stress tensor and strain tensor as:

$$\begin{cases} \sigma_{xx} = \lambda\varepsilon_v + 2\mu\varepsilon_{xx} \\ \sigma_{yy} = \lambda\varepsilon_v + 2\mu\varepsilon_{yy} \\ \sigma_{zz} = \lambda\varepsilon_v + 2\mu\varepsilon_{zz} \\ \sigma_{xy} = \mu\varepsilon_{xy} \\ \sigma_{xz} = \mu\varepsilon_{xz} \\ \sigma_{yz} = \mu\varepsilon_{yz} \end{cases} \tag{18}$$

Expending Eq. (18) yields a relationship between the stress & its rate and the strain & its rate as Eq. (19).

$$\begin{cases} \sigma_{xx} + \tilde{\upsilon}\dot{\sigma}_{xx} = \lambda\varepsilon_v + 2\mu\varepsilon_{xx} + \tilde{\lambda}\dot{\varepsilon}_v + 2\tilde{\mu}\dot{\varepsilon}_{xx} \\ \sigma_{yy} + \tilde{\upsilon}\dot{\sigma}_{yy} = \lambda\varepsilon_v + 2\mu\varepsilon_{yy} + \tilde{\lambda}\dot{\varepsilon}_v + 2\tilde{\mu}\dot{\varepsilon}_{xx} \\ \sigma_{zz} + \tilde{\upsilon}\dot{\sigma}_{zz} = \lambda\varepsilon_v + 2\mu\varepsilon_{zz} + \tilde{\lambda}\dot{\varepsilon}_v + 2\tilde{\mu}\dot{\varepsilon}_{zz} \\ \sigma_{xy} + \tilde{\upsilon}\dot{\sigma}_{xy} = \mu\varepsilon_{xy} + \tilde{\mu}\dot{\varepsilon}_{xy} \\ \sigma_{xz} + \tilde{\upsilon}\dot{\sigma}_{xz} = \mu\varepsilon_{xz} + \tilde{\mu}\dot{\varepsilon}_{xz} \\ \sigma_{yz} + \tilde{\upsilon}\dot{\sigma}_{yz} = \mu\varepsilon_{yz} + \tilde{\mu}\dot{\varepsilon}_{yz} \end{cases} \tag{19}$$

where, $\tilde{\upsilon}$, λ, μ, $\tilde{\lambda}$ and $\tilde{\mu}$ are the parameters of the material. The superscript '.' represents the rate of the variable. ε_v is the volume strain, defined as:

$$\varepsilon_v = \varepsilon_{xx} + \varepsilon_{yy} + \varepsilon_{zz} \tag{20}$$

The central different format is applied in this study to keep the numerical algorithm stable. The values of function f and rate of function f in the central point of the time t, i.e., $f_{t+\frac{1}{2}\Delta t}$ and $\dot{f}_{t+\frac{1}{2}\Delta t}$, are defined in Eq. (21), respectively.

$$\begin{cases} \dot{f}_{t+\frac{1}{2}\Delta t} = \dfrac{\Delta f}{\Delta t} \\ f_{t+\frac{1}{2}\Delta t} = f_t + \dot{f}_{t+\frac{1}{2}\Delta t} \cdot \dfrac{1}{2}\Delta t = f_t + \dfrac{\Delta f}{2} \end{cases} \tag{21}$$

where, f_t and Δf represent values of the unknown function f and increment of the unknown function f in the time t.

Utilize Eq. (21) to fabricate the updated formula of the constitutive equation in the time t, defined as Eq. (22).

$$\begin{cases} \Delta t\sigma_{xx}^{t}+(\dfrac{\Delta t}{2}+\tilde{\upsilon})\Delta\sigma_{xx}^{t}=2\mu\Delta t\varepsilon_{xx}^{t}+\Delta t\lambda\varepsilon_{v}^{t}+(\Delta t\mu+2\tilde{\mu})\Delta\varepsilon_{xx}^{t}+(\Delta t\dfrac{\lambda}{2}+\tilde{\lambda})\Delta\varepsilon_{v}^{t} \\ \Delta t\sigma_{xy}^{t}+(\dfrac{\Delta t}{2}+\tilde{\upsilon})\Lambda\sigma_{xy}^{t}=\Lambda t\mu\varepsilon_{xy}^{t}+(\Lambda t\dfrac{\mu}{2}+\tilde{\mu})\Lambda\varepsilon_{xy}^{t} \end{cases} \tag{22}$$

And the components of the Jacobi Matrix contributing to the coverage during the iteration procedure are deduced as Eq. (23).

$$\begin{cases} \dfrac{\partial\Delta\sigma_{xx}}{\partial\Delta\varepsilon_{xx}}=\dfrac{\partial\Delta\sigma_{yy}}{\partial\Delta\varepsilon_{yy}}=\dfrac{\partial\Delta\sigma_{zz}}{\partial\Delta\varepsilon_{zz}}=\dfrac{1}{\dfrac{\Delta t}{2}+\tilde{\upsilon}}[\Delta t(\dfrac{\lambda}{2}+\mu)+\tilde{\lambda}+2\tilde{\mu}] \\ \dfrac{\partial\Delta\sigma_{xx}}{\partial\Delta\varepsilon_{yy}}=\dfrac{1}{\dfrac{\Delta t}{2}+\tilde{\upsilon}}[\Delta t(\dfrac{\lambda}{2})+\tilde{\lambda}] \\ \dfrac{\partial\Delta\sigma_{xx}}{\partial\Delta\varepsilon_{zz}}=\dfrac{1}{\dfrac{\Delta t}{2}+\tilde{\upsilon}}[\Delta t(\dfrac{\lambda}{2})+\tilde{\lambda}] \\ \dfrac{\partial\Delta\sigma_{xy}}{\partial\Delta\varepsilon_{xy}}=\dfrac{\partial\Delta\sigma_{xz}}{\partial\Delta\varepsilon_{xz}}=\dfrac{\partial\Lambda\sigma_{yz}}{\partial\Delta\varepsilon_{yz}}=\dfrac{1}{\dfrac{\Delta t}{2}+\tilde{\upsilon}}[\Delta t(\dfrac{\mu}{2})+\tilde{\mu}] \end{cases} \tag{23}$$

It is too complex and involved to use Eq. (23) to update the Jacobi Matrix in the whole creep analysis procedure. Furthermore, the numerical results even depend on the increment of the time in some conditions [48].

When the force loading with Heaviside function is implemented for testing the creep response, the Jacobi Matrix including the time influence is required to be employed as Eq. (24). It should be mentioned that which Jacobi Matrix is more rigorous and rational is still an involved topic in computational mechanics hitherto.

$$D=\begin{pmatrix} a_{11} & a_{12} & a_{13} & 0 & 0 & 0 \\ a_{21} & a_{22} & a_{23} & 0 & 0 & 0 \\ a_{31} & a_{32} & a_{33} & 0 & 0 & 0 \\ 0 & 0 & 0 & a_{44} & 0 & 0 \\ 0 & 0 & 0 & 0 & a_{55} & 0 \\ 0 & 0 & 0 & 0 & 0 & a_{66} \end{pmatrix} \tag{24}$$

where, a_{11} a_{22} and a_{33} equal to $\dfrac{1}{\dfrac{\Delta t}{2}+\tilde{\upsilon}}[\Delta t(\dfrac{\lambda}{2}+\mu)+\tilde{\lambda}+2\tilde{\mu}]$, a_{44}, a_{55} and a_{66}

equal to $\frac{1}{\frac{\Delta t}{2}+\tilde{\upsilon}}[\Delta t(\frac{\mu}{2})+\tilde{\mu}]$, a_{12}, a_{21}, a_{13}, a_{31}, a_{23} and a_{32} equal to $\frac{1}{\frac{\Delta t}{2}+\tilde{\upsilon}}[\Delta t(\frac{\lambda}{2})+\tilde{\lambda}]$.

When the damage occurs in material, Eq. (24) can be rewritten as:

$$D=(1-\omega)\begin{pmatrix} a_{11} & a_{12} & a_{13} & 0 & 0 & 0 \\ a_{21} & a_{22} & a_{23} & 0 & 0 & 0 \\ a_{31} & a_{32} & a_{33} & 0 & 0 & 0 \\ 0 & 0 & 0 & a_{44} & 0 & 0 \\ 0 & 0 & 0 & 0 & a_{55} & 0 \\ 0 & 0 & 0 & 0 & 0 & a_{66} \end{pmatrix} \tag{25}$$

When the visco-elastic damage property of material is considered, numerical method implementation is required from Eq. (17) to Eq. (25) for substituting the analytic solution from Eq. (6) to Eq. (12).

Actually, the analytic method becomes nonapplicable for obtaining the solution when the boundary condition becomes complex or in the 3D state, where the numerical method plays a leading role. For expanding the application of the proposed constitutive model (Eq. (25)), a user defined material subroutine（short for UMAT） written in Fortran language is integrated into the FEM software. The constitutive model is complied with the flow as shown in the Fig. 3. Assume that the analysis has been executed for n^{th} loops, and the $n+1^{th}$ loops will commence. The time and time increment in the n^{th} loops are t and Δt, respectively.

(1) Obtain the strain increment $\Delta\varepsilon_{ij}^{n+1}$ and the time increment Δt^{n+1} provided by FEM result at the $n+1^{th}$ loops; the strain components ε_{ij}^{n} and the stress components σ_{ij}^{n} provided by FEM result at the n^{th} loops;

(2) Calculate the pseudo stress components σ_{ij}^{n+1} at the $n+1^{th}$ loops based on Eq. (22);

(3) Update the equivalence stress at the $n+1^{th}$ loops based on Eqs. (7-8);

(4) Update the equivalence damage variable at the $n+1^{th}$ loops based on Eq. (13);

(5) Recalculate and update the stress components σ_{ij}^{n+1} at the n+1th loops based on Eq. (12) considering the damage factor;

(6) Update the Jacobi Matrix;

(7) Jump out of the subroutine and return to the main program.

4 Validation on the proposed 3D visco-elastic coupled damage constitutive model

4.1 Uniaxial compression test

The uniaxial compression experiment is usually utilized to describe the creep behavior of asphalt concrete [49]. A series of uniaxial compression numerical tests using the visco-elastic model coupled with K-R damage theory are simulated under loads with different magnitudes. The three-stage creep characteristics of the asphalt and asphalt concrete are very crucial for numerical procedure with FEM. Parameters defining the visco-elastic constitutive and damage evolution are listed in Table 1 [40].

The numerical creep curves of specimens under the uniaxial compression are found matching well with the experimental data [40] with variations less than 5%, as shown in Fig 4. An outstanding advantage of the proposed model over traditional ones [32, 40] is that this model can keep numerical and experimental results close while maintaining all inputs constant under different loading magnitudes except $\tilde{\upsilon}$. $\tilde{\upsilon}$ is utilized for defining the initial elastic instantaneous response. The visco-elastic damage model in this paper is simply and effective for the design and analysis on asphalt and asphalt concrete material and structure under compression.

From Fig.4, the three-stage creep behavior can be observed both in the numerical and experimental results under conditions when the compressive loading higher than 0.20MPa. Such three-stage creep behavior was not found under 0.10MPa loading magnitude. The reason can be explained as that when the loading magnitude is not high enough or the loading time is not long enough, the accelerated creep failure phenomenon will not exhibit obviously. The accelerated creep failure can be barely observed under 0.15MPa compressive loading magnitude. When the loading time increases, the third stage, i.e. accelerated creep failure, can be observed even the loading magnitudes are small, 0.10MPa and 0.15MPa, as shown in Fig. 5.

Comparison between Fig. 4 and Fig. 5 indicates that the larger the compressive loading, the faster the third stage creep behavior of asphalt concrete occurs.

Indeed, under the vehicle loading magnitude, which is often smaller than those used in the uniaxial compression, the asphalt and asphalt concrete will manifest the accelerated creep sooner or later in the in-situ performance, in which the loading is approximate repeated with the lower loading magnitude, longer loading time and changing temperature. It can be claimed that asphalt and asphalt concrete will be markablely dominated and mediated by the loading magnitude. Furthermore, the loading time is also involved in the formation the accelerated creep failure besides the ambient temperature. The total creep behaviors of asphalt in the numerical test are exhibited with prolonged step times, as shown in Fig.5. This model predicts that the creep time can activate the accelerated creep failure. The loading magnitude, however, is unable to activate the creep accelerated failure due to not enough sustained loading time. Actually, the damage mechanism is expected to prompt the formation of the creep accelerated failure by inducing the degradation of stiffness by considering the statistical influence of the interaction and intersection of craze arising in the meso and micro scales [50]. This intrinsic phenomenon provides the proof that long time may be the most important factor for the accelerate creep behavior due to the essence of the rheology property of the asphalt and asphalt concrete [51-52].

The damage evolution curves under different loading magnitudes are shown in Fig.6. Similar tendencies were observed on the creep strain. Fig. 6 supports the concept that the damage mechanism is critical for the formation of the accelerated creep stage, and the damage evolution influences the service life of asphalt and asphalt concrete material [53-54].

4.2 Pre-notched three-point bending beams test

The applicability of the proposed 3D visco-elastic coupled damage constitutive model on bending mode was investigated through the pre-notched three-point bending beam test. Compared with the direct tension test, the indirect tension test and the semi-circular bending test, the three-point bending beams are easy to prepare without

inducing the defects [55-57]. The geometry size of the beam is shown in Fig.7. The length, depth, and height are 300mm, 50mm, and 80mm, respectively. An initial notch was fabricated in the middle of the beam bottom. The width and height of notch are 2mm and 20mm, respectively. The MTS system was used to apply a 20mm/min load on the indenter, and two rolling supports provided the reaction forces.

In the FEM model (Fig. 8), pre-notched beams were created. Considering the converge problem due to the singularity on the crack tip, a semi-circle with 1mm radius was assumed for the crack tip in the FEM model. 4000 four-node plane stress elements were utilized. The boundary condition is similar to the experiment. There are two rolling supports providing fixed displacement constraints in the X and Y directions without the rolling constraints, and the top indenter is implemented with a 20mm/min velocity load. The parameters utilized in the model are listed in Table 2.

The load-crack mouth opening displacement (P-CMOD) curve is usually a measurement to compare numerical simulation and laboratory test [58-59]. From Fig. 9, it is found that the numerical and experimental P-CMOD curves match well. In order to further explore the fracture mechanism, the Von-Mises contour of the three point bending beam in the ultimate fracture stage is shown in Fig. 10, as well as the normal stress and strain contours in the X and Y directions shown in Fig. 11, and damage contour shown in Figs. 12. An intensity distribution region of the Von-Mises equivalence stress exists on the tip of the initial notch forming a branch pattern along about 30 degree with the Y direction, and the magnitude of the Von-Mises equivalence stress is around 5.7kPa (Fig. 10). Similar results can be observed in the normal stress and strain contours in the X direction (Fig. 11).

The magnitude of the normal stress in the X and Y directions are 5.3kPa and 2.3kPa, respectively, which proves that the beam is mainly under tension state. In the three-point bending beam test for cement concrete, the ratio of the normal stress magnitudes in the X and Y directions in the final fracture step ranges from 10 to 20 times [35]. According to Fig. 11, the ratios of the magnitudes of the normal stress and normal strain in the X and Y directions are only 2 times and 6 times, respectively. It can be claimed that stress levels in the two directions are comparable to each other,

and both can influence the damage evolution. Thus, the uniaxial stress condition is not the real case when asphalt concrete is in fracture failure. The 3D visco-elastic damage model is critical and necessary for predicting the damage behavior of asphalt and asphalt concrete. The damage distribution contour (Fig. 12) also has the similar intensity region with that in the Von-Mises equivalence stress contour (Fig. 10), as the Von-Mises equivalence stress contributes the evolution of the damage variable. According to the damage distribution contour in Fig. 12, the most probable fracture path was drew manually out with an oblique line. Fig. 13 shows the fracture path in the pre-notched three-point bending beam test. It is found that the fracture path will propagate generally along with the loading axial, which is similar to the damage distribution in the numerical simulation (Fig. 12). Therefore, the efficiency and accuracy of the numerical method are acceptable when simulating the fracture and failure of asphalt concrete under complex loading conditions.

Bending is a main loading mode in the birth of distresses such as rutting and fatigue cracking on asphalt pavement. Asphalt pavement layer(s) is closer to the plane structure. The stress state in the middle and the profile of the asphalt pavement layers always manifest the difference, being the plane stress state and the plane strain state respectively. The three-point bending beam test need to reflect this kind of transition in stress state. Without considering this transition, the three-point bending beam test will not provide the satisfactory information for the bending mode of asphalt pavement.

Three-point bending beams with different depths (50mm, 75mm, and 125mm) were casted and the bending tests were conducted in laboratory. The length and height of the beams are the same, 300mm and 80mm, respectively. The corresponding simulations were conducted using the proposed model. Fig. 14 shows the P-CMOD curves of the experimental and simulated results. It can be seen that the failure strengths in simulation match well with experimental results, indicating the proposed model is applicable to describe beam bending with varied depths, i.e., beams either in plate stress or plate strain states or 3D load states. The difference between measured and simulated P-CMOD curves may be due to the random distribution of aggregates

surrounding pre-notches in the beams in experiments.

In order to study the influence of the beam depth on the bending behavior of asphalt mixture, pre-notched three-point bending beams with various depths (10% to 90% of the unit depth, 50mm) were built and the bending tests were simulated in the proposed model with keeping the rest inputs constant. Fig. 15 shows the numerical P-CMOD curves. It can be seen that the failure strength increases as the beam depth increases. Additionally, the softening behaviors of beams with different depths are different. In specific, the thicker the beam, the faster the reaction force drops after the failure, which can be explained as follows: (1) the more area of asphalt mixture reaches the material's stress limit, the higher the failure strength. (2) However, once the softening behavior starts, beams with higher depths have larger unloading areas than the ones with smaller depths, releasing more energy. Similar phenomena were observed in Cao et al. [33].

5. Conclusions

In this study, a novel visco-elastic damage model (2S1D model) was proposed. The three stages of creep behavior of the asphalt and asphalt concrete was described with the K-R creep damage theory, which was then implemented into the novel visco-elastic damage model to simulate failure mechanism of such materials in ABAQUS platform with a self-developed UMAT. Based on numerical tests and lab experiments, we can draw conclusions as follows:

(1) The good consistence between numerical and experimental results indicates validity and effectiveness of the proposed visco-elastic damage model.

(2) An advantage of the proposed visco-elastic damage model is that merely one parameter of the model needs to be reset for fitting the experimental results in the different loading magnitudes while the parameters related to the damage evolution behavior keep constant from case to case. This merit is of crucial importance in practice and suitable for the large-scale computation. Another advantage is that the FEM model using the proposed constitutive model can simulate the damage evolution of asphalt and asphalt concrete without serious converge problems.

(3) Even under low loading magnitudes the asphalt and asphalt concrete still inevitably enter the accelerated creep stage when the loading time is long enough.

(4) The uniaxial visco-elastic damage constitutive model fails to describe the failure phenomenon of asphalt concrete, yielding developing 3D visco-elastic damage constitutive models necessary.

(5) The proposed model is applicable to simulating the three-point bending beams with varied depths, i.e., beams either in plate stress or plate strain states or in 3D load states.

(6) In the three-point bending test, the failure strength increases as the beam depth increases. Specifically, the thicker the beam, the faster the reaction force drops after the failure.

Acknowledgements

This work was financially supported by the National Natural Science Foundation of China (51769028, 51508137), the Key Research and Development Projects in Hainan Province (ZDYF2017100), Natural Science Foundation of Qinghai Province of China (2017-ZJ-933Q), Beijing Institute of Structure and Environment Engineering Fund (BQ2019001), and Fundamental Research Funds for the Central Universities (DUT20JC50 and DUT17RC(3)006).

Reference

[1] Bhasin A, Bommavaram R, Greenfield M L, Little D. Use of molecular dynamics to investigate self-healing mechanisms in asphalt binders. J. Mater. Civ. Eng., 2011; 23: 485-492.

[2] Redelius P, Soenen H. Relation between bitumen chemistry and performance. Fuel. 2015; 140: 34-43.

[3] Lesueur D. The colloidal structure of bitumen: Consequences on the rheology and on the mechanisms of bitumen modification. Adv Colloid Interface Sci. 2009; 145 (1-2): 42-82.

[4] Alfrey T. Mechanical behavior of high polymers. Interscience publishers, New York. 1948.

[5] Mark J E. Physical Properties of Polymers. American Chem Soc. Washington D.C.

1984.

[6] D'Angelo J A, Fee F. Superpave binder tests and specifications: How have they performed in the real world. Asphalt Paving Technol., 2000; 7: 697-713.

[7] Masad E, Somadevan N. Microstructural Finite-Element Analysis of Influence of Localized Strain Distribution on Asphalt Mix Properties. Journal of Engineering Mechanics, 2002; 10, 1105-1114.

[8] Moreno F, Rubio M C. Effect of aggregate nature on the fatigue-cracking behavior of asphalt mixes. Mat Design. 2013; 47: 61-67.

[9] Gross B. Mathematical structure of the theories of viscoelasticity. Hermann. Paris. 1953.

[10] Wang H, Zhu K, Yan Z. A practical creep compliance model of asphalt mixtures and its application. Acta Mechanica Solida Sinica. 2002; 23 (2): 232-236.

[11] Cai Y, Ye Y. Experimental researches on viscoelastic behavior of asphalt sand mixture. Engr. Mech. 2010; 27(Suppl I): 200-204.

[12] Zhan X, Zhang X, Wang D, Lu L. Study on nonlinear viscoelastic constitutive equation of modified asphalt and its applications. Engr. Mech. 2009; 26(4): 187-191.

[13] Wu J. Uniaxial compression creep prediction of asphalt mixture using the Eshelby equivalent inclusion method. Adv Mater Res, 2014, 1061-1062: 410-413.

[14] Xiao S, Zhou X, Hu X, Luo W. Linear rheological solid model with fractional derivative and its application. Engr. Mech. 2009; 29(10): 354-358.

[15] Zhang C, Zhang W. Research progresses on nonlinear viscoelasticity and its applications. Natural Science Journal of Xiangtan University. 2003; 25(4): 28-32.

[16] Pasetto M, Baldo N. Numerical visco-elastoplastic constitutive modelization of creep recovery tests on hot mix asphalt. J Traffic Transport Eng. 2016, 3(5): 390-397.

[17] Xu M, Tan W. Representation of the constitutive equation of viscoelastic materials by the generalized fractional element networks and its generalized solutions. Science in China Series G: Physics Mechanics and Astronomy. 2003; 46(2): 145-157.

[18] Deshpande V S, Cebon D. Steady-State Constitutive Relationship for Idealized Asphalt Mixtures. Mech. Mater., 1999; 31: 271-287.

[19] Flaceliere L, Morel F, Dragon A. Competition between mesoplasticity and

damage under HCF -elasticity/damage shakedown concept. Int. J. Fatigue. 2007; 29: 2281-2297.

[20] Perzyna P. Fundamental problems in viscoplasticity. Adv Appl Mech. 1966; 9: 243-377.

[21] Kim Y R, Little D N. Linear viscoelastic analysis of asphalt Mastics. J. Mater. Civ. Eng. 2004; 16 (2): 122-132.

[22] Park S W, Kim Y R, Schapery R A. A viscoelastic continuum damage model and its application to uniaxial behavior of asphalt concrete. Mech. Mater. 1996; 24(4): 241-255.

[23] Darabi M K, Abu Al-Rub R K, Masad E A, Huang C, Little D N. A thermo-viscoelastic-viscoplastic-visco damage constitutive model for asphaltic materials. Int. J. Solids Struct. 2011; 48(1): 191-207.

[24] Darabi M K, Abu Al-Rub R K, Masad E A, Little D N. Thermodynamic‐based model for coupling temperature‐dependent viscoelastic, viscoplastic, and viscodamage constitutive behavior of asphalt mixtures. Int. J. Numer. Anal. Met Geomech. 2012, 36(7): 817 – 854.

[25] Shahsavari H, Naghdabadi R, Baghani M, Sohrabpour S. A viscoelastic–viscoplastic constitutive model considering damage evolution for time dependent materials: Application to asphalt mixes. Int J Damage Mech, 2016, 25(7): 921-942.

[26] Judycki J. Non-linear viscoelastic behavior of conventional and modified asphaltic concrete under creep. Mater. Struct. 1992; 25(1): 95-101.

[27] Zhang J, Pei J, Wang B. Research on Time-Temperature-Stress Equivalence Principle For Asphalt Mixture. ASC: ICCTP2010, 2010; 3516-3520.

[28] Zhang J, Huang X. Viscoelastic model for asphalt mixture under repeated haversine load. J. Southeast Univ. (English Edition). 2009; 25(4): 523-526.

[29] Zheng J, Tian X, Ying R. A laboratory research on the thermo-viscoelastic constitutive model of bituminous mixture. J. Changsha Univ. Sci. Tech.: Natural Sci. Edition. 2004; 1(1): 1-7.

[30] Zheng J, Lyu S, Tian X. Viscoelastic damage characteristics of asphalt based on creep test. Engr. Mech. 2008; 25(2): 193-196.

[31] Lu Y, Wright P J. Numerical approach of visco-elastoplastic analysis for asphalt mixtures. Comput. Struct. 1998; 69(2): 139-147.

[32] Ye Y, Yang X, Chen C. Experimental Researches on visco-elastoplastic Constitutive Model for Asphalt Mastic. Constr. Build Mater. 2009; 23(10): 3151-3165.

[33] Ye Y, Yang X, Chen C. Modified Schapery's model for asphalt sand. J Engr. Mech. 2010; 136(4): 448-454.

[34] Cao P, Feng D, Zhou C. A Modified Damage-Plasticity Coupled Area-Weighted Nonlocal Model for Simulating Ductile Fracture and Softening Behaviors of Materials, Math Prob Engr., 2014; Article ID 862543.

[35] Cao P, Feng D, Zhou C. Study on Fracture Behavior of Polypropylene Fiber Reinforced Concrete Utilizing Three-Point Bending Beam Test. Comput. Concr. 2014; 5(14): 527-546.

[36] Bandyopadhyaya R, Das A, Basu S. Numerical simulation of mechanical behavior of asphalt mix. Constr. Build. Mater. 2008; 22(6): 1051-1058.

[37] AASHTO T321. Standard method of test for determining the fatigue life of compacted asphalt mixtures subjected to repeated flexural bending. 2017.

[38] Hafeez I, Kamal M A, Mirza M W, Bilal S. Laboratory fatigue performance evaluation of different field laid asphalt mixtures. Constr. Build. Mater. 2013; 44: 792-797.

[39] Castro M, Sanchez J A. Estimation of asphalt concrete fatigue curves- a damage theory approach. Constr. Build. Mat. 2008; 22: 1232-1238.

[40] Zeng G, Yang X, Bai F, Yin A. Experimental researches on a visco-elastoplastic creep damage constitutive model of asphalt mastic. Engr. Mech. 2013; 30(4): 249-253.

[41] Bergstrom, J.S. Mechanics of Solid Polymers: Theory and computational modeling; William Andrew: Burlington, MA, USA, 2015.

[42] Yu S, Feng X. Damage mechanics. Beijing: Tsinghua University Press. 1997.

[43] Kachanov L M. Introduction to continuum damage mechanics. J. Applied Mech. 1987; 54(2): 481.

[44] Rabotnov Y. N. On the equation of state for creep. Progress in applied mechanics, 1963; 307-315.

[45] Cao, P. Elastic-plastic damage models and user-defined material subroutine in ABAQUS software of concrete. Master Thesis of Shenyang Univ. Tech., Shenyang, China 2009.

[46] Lemaitre J, Desmorat R. Engineering Damage Mechanics. Springer, Berlin

Heidelberg New York. 2005.

[47] Lemaitre J, Chaboche J.L. Mechanics of solid materials. Cambridge: Cambridge University Press. 1990.

[48] Simo J C, Hughes T J R. Computational inelasticity. New York: Springer, 2000; 162-168.

[49] Deshpande, V S, Cebon D. Uniaxial experiments on idealized asphalt mixtures. J Mater Civ Eng, 2000; 12(3): 262-71.

[50] Mohanraj J, Barton D C, Ward I M, Dahoun A, Hiver J M, G'Sell C. Plastic deformation and damage of polyoxymethylene in the large strain range at elevated temperatures. Polymer. 2006; 47: 5852-5861.

[51] Anderson D A. and Kennedy T W. Development of SHRP Binder Specification. J Assoc Asph Paving Tech, 1993; 62: 481-507.

[52] Marasteanu M. Emerging Methods in Asphalt Binder Rheological Characterization. Road Mater Pavement Design. 2007; 8(2): 257-284.

[53] Gu G, Xia Y, Lin C, Lin S, Meng Y, Zhou Q. Experimental study on characterizing damage behavior of thermoplastics. Mater Design. 2013; 44: 199-207.

[54] Varvani-Farahani A, Sharma M, Kianoush M R. Fatigue damage analysis and life assessment under variable amplitude loading conditions. Mater Sci Eng A. 2005; 403(1-2): 42-47.

[55] Molenaar A A A, Scarpas A, Liu X, Erkens S M J G. Semi-circular bending test; simple but useful? J Assoc Asphalt Paving Technol. 2002; 71: 794-815.

[56] EN12697-44. Bituminous mixtures. Test methods for hot mix asphalt. Crack propagation by semi-circular bending test. 2010.

[57] Vervuurt A, Schlangen E, Van Mier J G M. Tensile cracking in concrete and sandstone: Part1--basic instruments. Mater. Struct., International Union of Laboratories and Experts in Construction Materials, Systems and Structures (RILEM), 1996; 29(2): 9-18.

[58] RILEM Technical Committee 50. Determination of the fracture energy of mortar and concrete by means of three-point bend tests on notched beams. Mater. Struct. 1985; 18(4): 287-290.

[59] Tada H, Paris P C, Irwin G R. The stress analysis of cracks handbook. St. Louis, Missouri, USA：Paris Productions Incorporated, 1985; 102-110.

List of Tables

Table 1 The visco-elastic parameters utilizing in the uniaxial compression simulation

Table 2 The relation between the D_G^{3D} and Poisson's ratio

List of Figures

Fig.1 Three components visco-elastic solid model in uniaxial condition

Fig. 2 The diagram of effective strain

Fig. 3 Flow chart of visco-elastic coupled damage model subroutine

Fig. 4 Comparison between test and numerical for creep strain curve under different loading scales

Fig.5 Three phases creep strain curve under different 0.1MPa and 0.15 MPa loading Scale

Fig. 6 The damage evolution curve under five different loading scales

Fig. 7 The three-point bending beam specimen

Fig. 8 FEM model of the three point bending beam

Fig. 9 The compared between the numerical result and experiment result for CMOD curve

Fig. 10 The Von-Mises equivalence stress distribution contour at the final step fracture of the three point bending test

Fig. 11 The normal stress distribution contour in the X direction at the final step

Fig. 12 The normal stress distribution contour in the Y direction at the final step

Fig. 13 The normal strain distribution contour in the X direction at the final step

Fig. 14 The normal strain distribution contour in the Y direction at the final step

Fig. 15 The damage distribution contour at the final step

Fig. 16 The ultimate fracture of the three point bending test

Fig. 17 The comparison of P-CMOD curves with different depths between the experiment results and numerical results

Fig. 18 The load-crack mouth opening displacement curves for different depths of the beam

Table 1 The visco-elastic parameters utilizing in the uniaxial compression simulation

Loading Scale (MPa)	λ (MPa)	μ (MPa)	$\tilde{\lambda}$ (MPa/s)	$\tilde{\mu}$ (GPa/s)	$\tilde{\upsilon}$ (MPa/s)	m	n	a (10^{-12})	α
0.10	0.7	1.4	70	14000	14	-0.7	1.8	300	0
0.15	0.7	1.4	70	14000	9.0	-0.7	1.8	300	0
0.20	0.7	1.4	70	14000	7.8	-0.7	1.8	300	0
0.25	0.7	1.4	70	14000	7.0	-0.7	1.8	300	0
0.30	0.7	1.4	70	14000	6.5	-0.7	1.8	300	0

Table 2 The relation between the D_G^{3D} and Poisson's ratio

Poisson's ratio	D_E^{3D}	D_G^{3D}
$\nu=0.2$	1.45	1.03
$\nu=0.3$	1.43	0.93
$\nu=0.4$	1.35	0.80

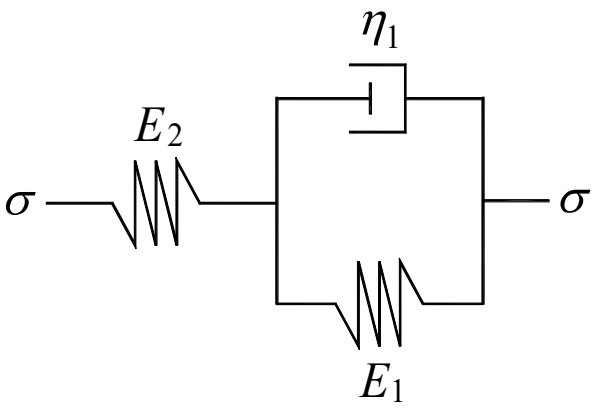

Fig.1 Three components visco-elastic solid model in uniaxial condition

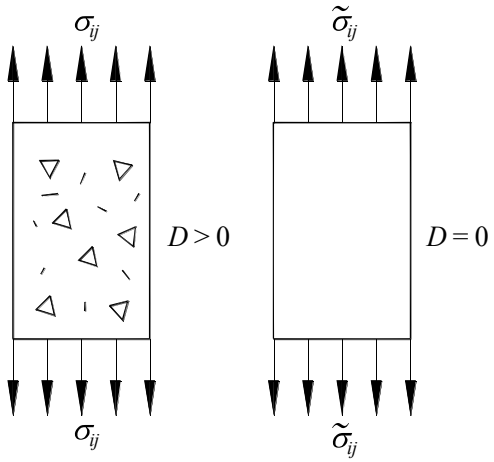

Fig. 2 The diagram of effective strain

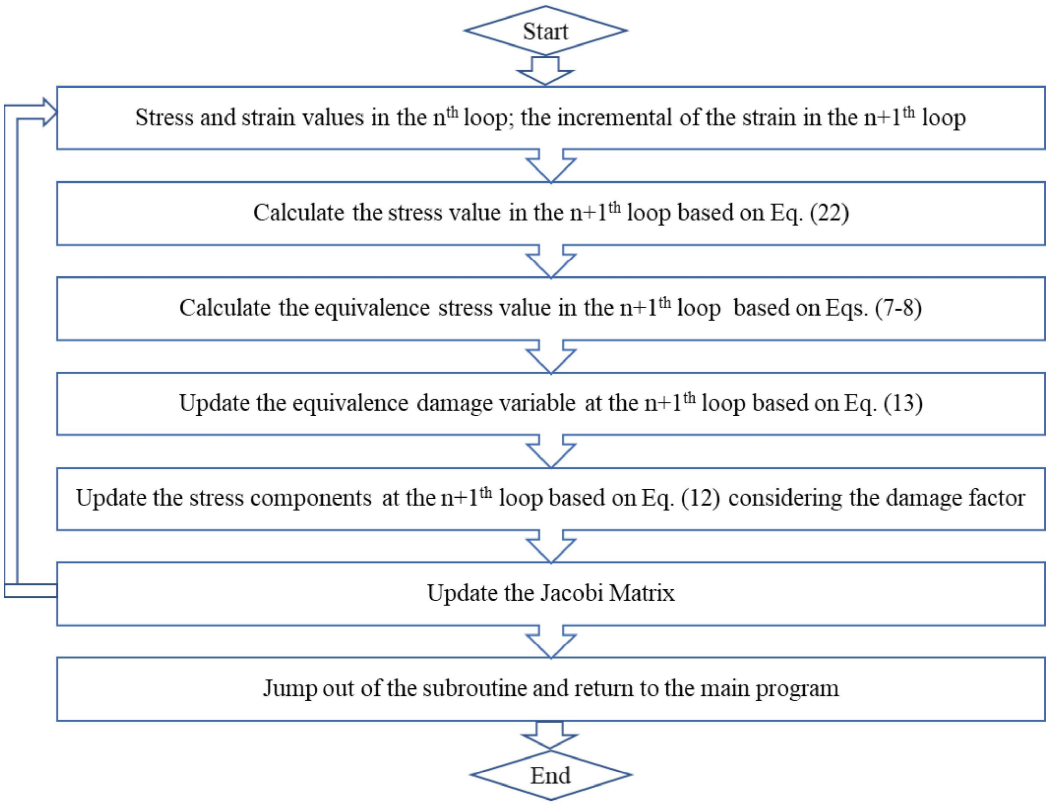

Fig. 3 Flow chart of visco-elastic coupled damage model subroutine

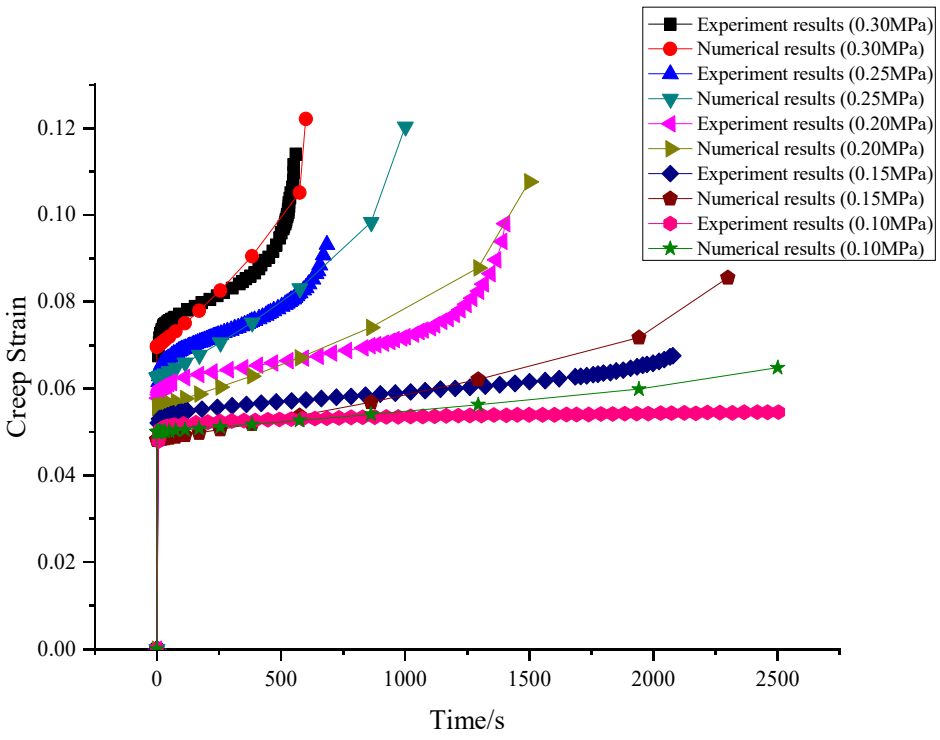

Fig. 4 Comparison between test and numerical for creep strain curve under different loading scales

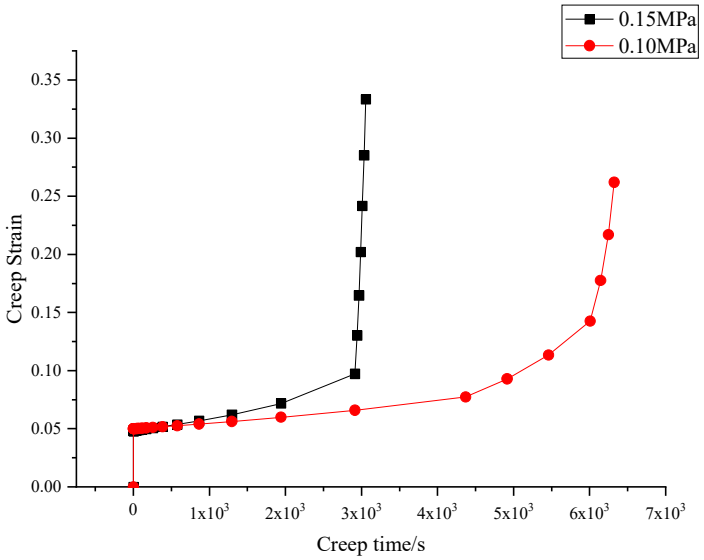

Fig.5 Three phases creep strain curve under different 0.1MPa and 0.15 MPa loading scale

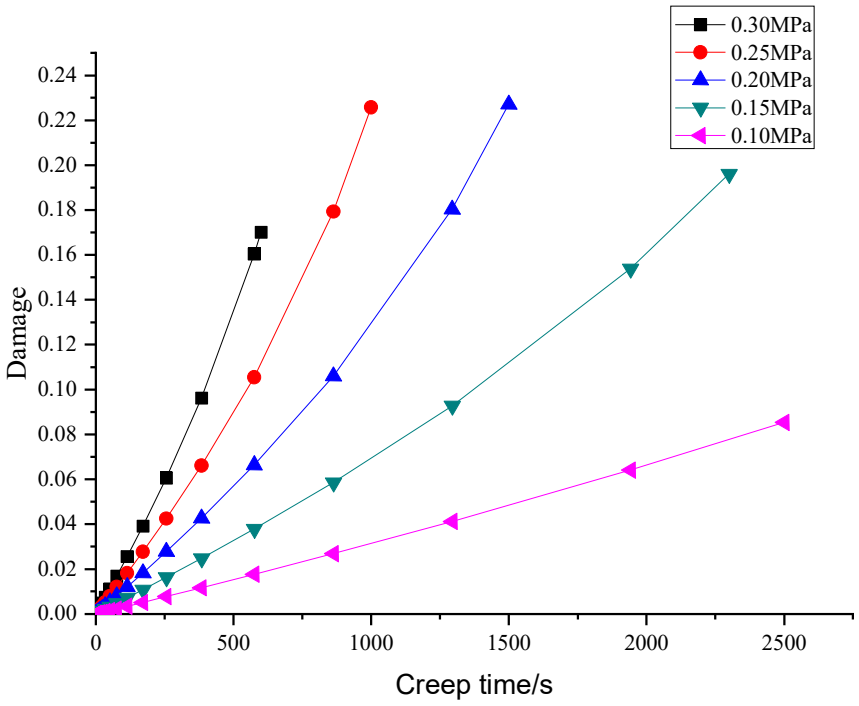

Fig. 6 The damage evolution curve under five different loading scales

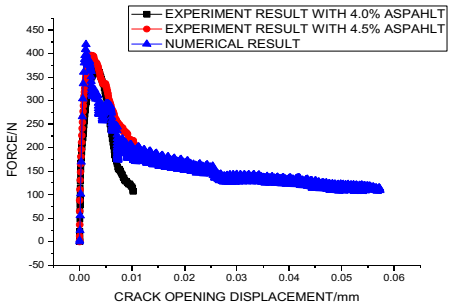

Fig. 7 The three-point bending beam specimen

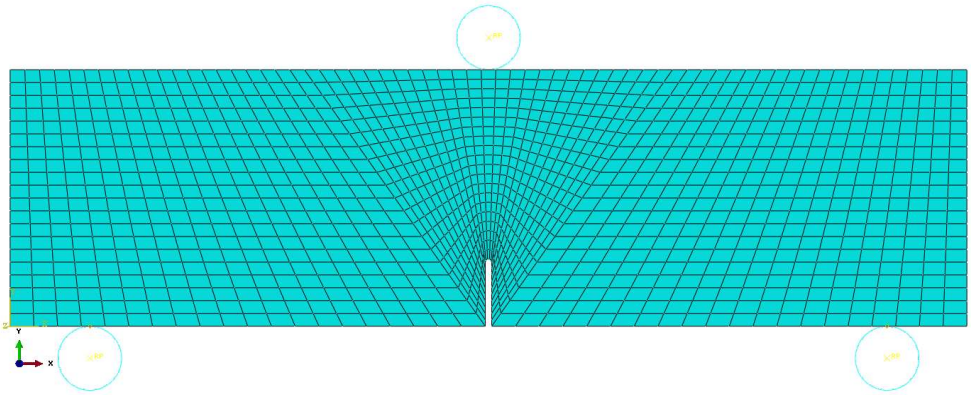

Fig. 8 FEM model of the three point bending beam

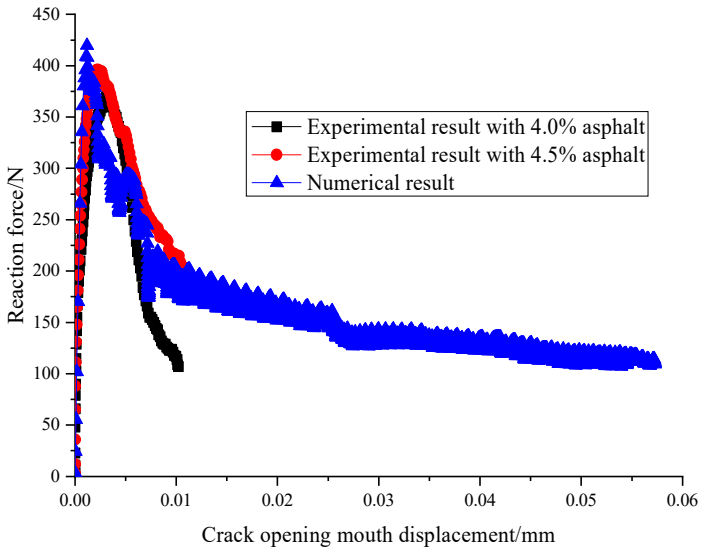

Fig. 9 The compared between the numerical result and experiment result for CMOD curve

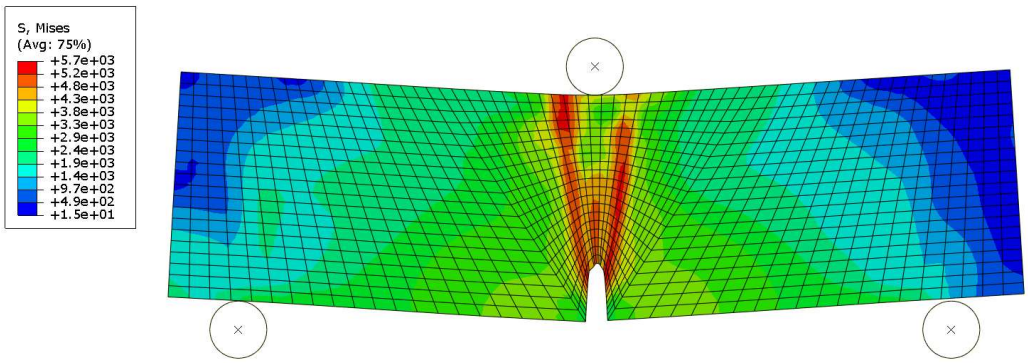

Fig. 10 The Von-Mises equivalence stress distribution contour at the final step fracture of the three point bending test

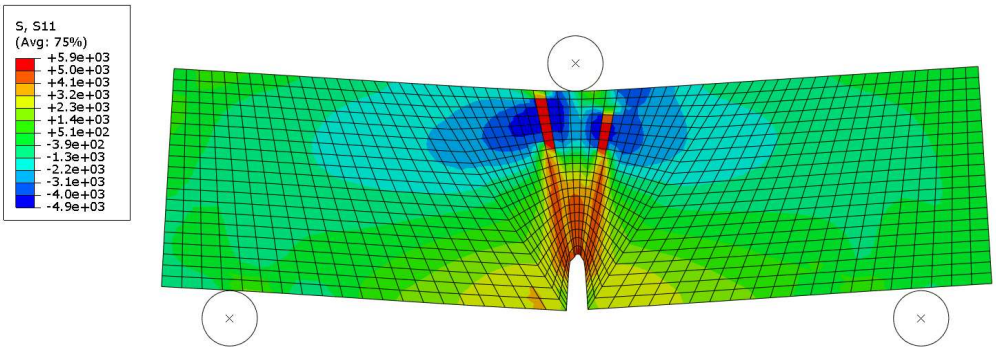

(a) the normal stress distribution contour in the X direction

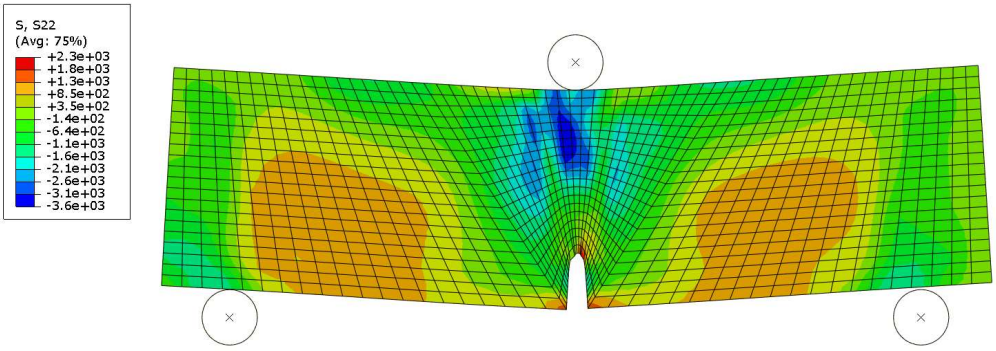

(b) The normal stress distribution contour in the Y direction

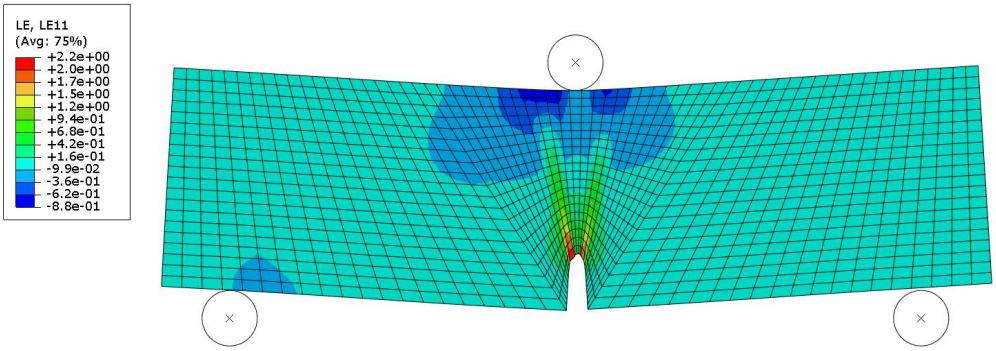

(c) the normal strain distribution contour in the X direction

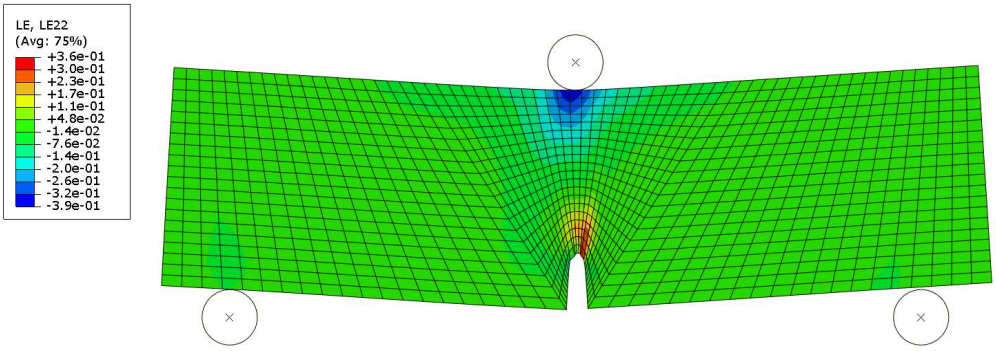

(d) the normal strain distribution contour in the Y direction

Fig. 11 The normal stress and strain distribution contours at the final step

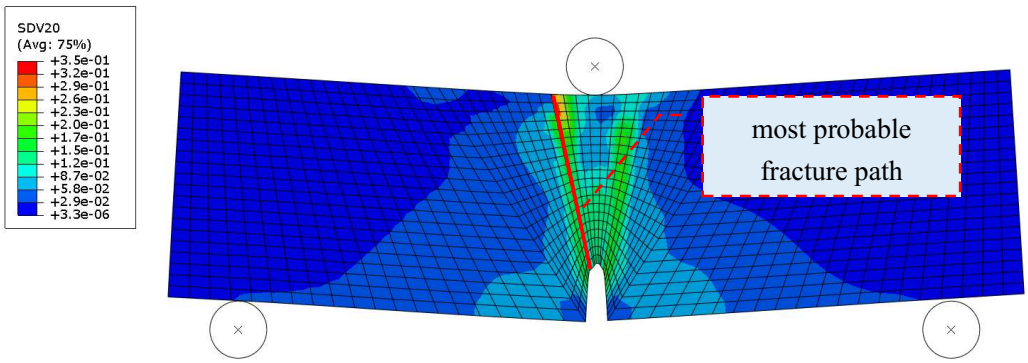

Fig. 12 The damage distribution contour at the final step

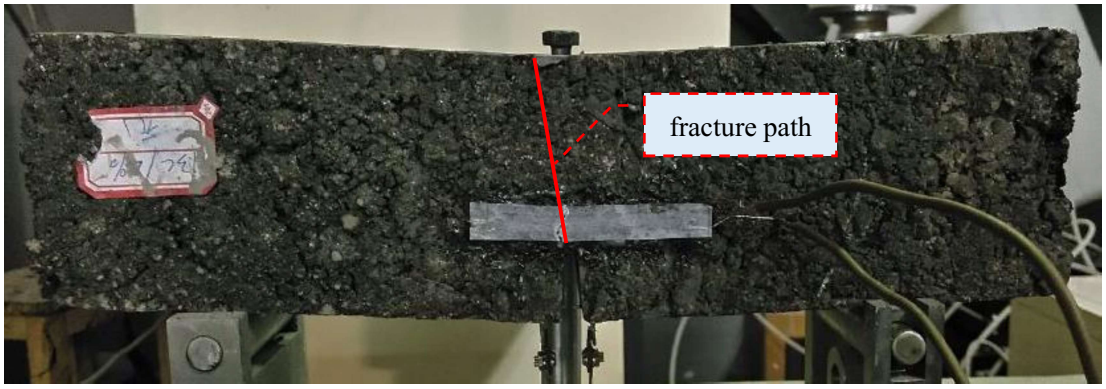

Fig. 13 The ultimate fracture of the three point bending test

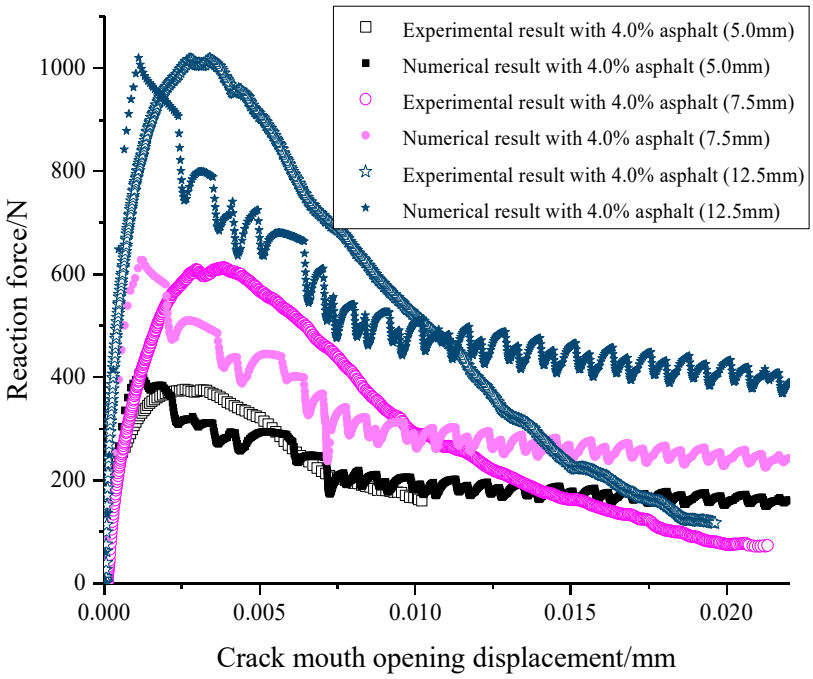

Fig. 14 The comparison of P-CMOD curves with different depths between the experiment results and numerical results

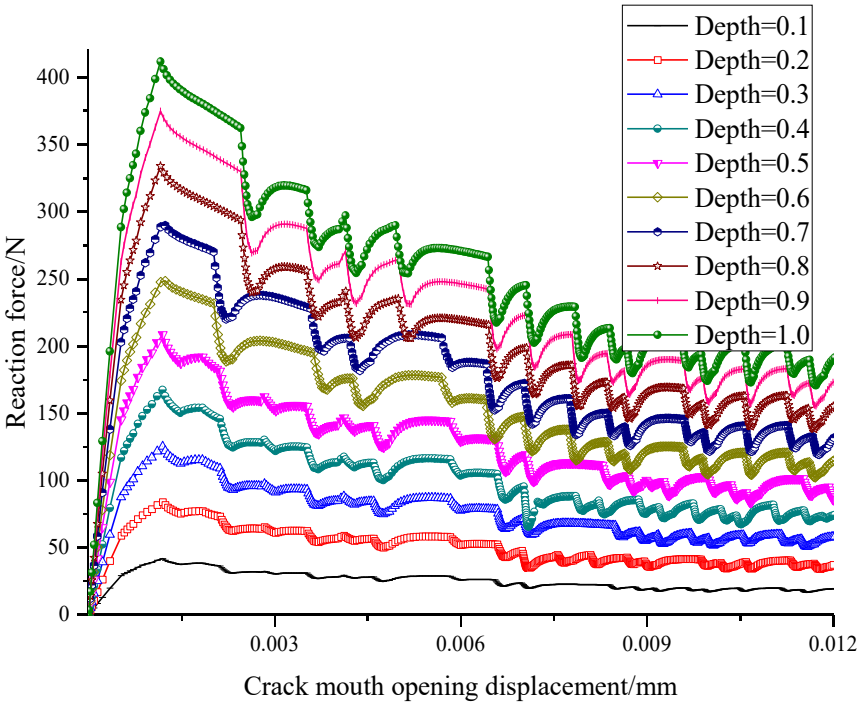

Fig. 15 The load-crack mouth opening displacement curves for different depths of the beam/m